A unified approach to acoustical reflection imaging. III: Extension to the elastic situation

C. P. A. Wapenaar and A. J. Berkhout
Delft University of Technology, Laboratory of Seismics and Acoustics, P.O. Box 5046, 2600 GA Delft, The Netherlands

The forward model, as derived in part I [A. J. Berkhout, J. Acoust. Soc. Am. **93**, 2005–2016 (1993)], and the inversion scheme, as derived in part II [A. J. Berkhout and C. P. A. Wapenaar, J. Acoust. Soc. Am. **93**, 2017–2023 (1993)], are extended to the elastic situation. The elastic forward and inverse problem are formulated in terms of matrices, similar as in the acoustic situation. Unlike in the acoustic situation, the matrices involved in the elastic problem each consist of 3×3 submatrices. For instance, the submatrices of the multi-component data matrix **V** represent single-component data matrices, each submatrix being related to a specific combination of source and receiver components. On the other hand, the submatrices of the multi-wavetype reflection matrix $\mathbf{R}^{\pm}$ represent single-wavetype reflection matrices, each submatrix being related to a specific combination of incident and reflected wavetypes. In the discussion of the elastic forward model the multi-component data matrix **V** at the acquisition surface is related to the multi-wavetype reflection matrices $\mathbf{R}^{\pm}$ in the subsurface. In the discussion of the inversion scheme it is shown how $\mathbf{R}^{\pm}$ is obtained step by step from the multi-component data matrix **V**. Once the multi-wavetype reflection matrices $\mathbf{R}^{\pm}$ have been determined the medium parameters can be much better resolved than in the acoustic situation.

PACS numbers: 43.60.Gk, 43.20.Gp

INTRODUCTION

The forward model for acoustic reflection measurements (Berkhout,[1] hereafter referred to as paper I) as well as the acoustical imaging approach (Berkhout and Wapenaar,[2] hereafter referred to as paper II) are strictly valid only for fluid media that cannot support shearing forces. In medical diagnostics the medium under investigation consists of human tissues that contain 90% water, hence the acoustical imaging approach is fully justified. In seismic exploration the geologic layers below the Earth's surface are of interest; they consist of solid rocks. Although for this situation the acoustical approach is not strictly valid, it is in many cases applied successfully by the seismic industry in the search for oil and gas. This success is explained by the fact that in relatively simple situations (small source–receiver offsets, low contrasts, simple geological structures) the acoustic wave equation describes reasonably well the propagation and reflection of compressional waves in solid media. In more complex situations, however, the acoustic approach breaks down and a full elastic extension of the imaging approach is needed. This is even more true for ultrasonic inspection of construction materials where shear waves carry a major part of the information on defects that need be imaged.

In this contribution we will extend the theory of papers I and II to the full elastic situation. As mentioned above, the main applications of full elastic imaging are in advanced seismic exploration and in ultrasonic inspection. To deal with both fields of application, we will set up the theory for complex media with an arbitrary inhomogeneous background medium (macro model), bounded above by a free (i.e., perfectly reflecting) acquisition surface and bounded below by a strong reflector (Fig. 1). For seismic exploration applications the background medium may be complex but the theory may be simplified by ignoring the effects of the strong bottom reflector. On the other hand, for many ultrasonic inspection situations the background medium may be taken homogeneous, but the bottom reflector plays a significant role.

I. MOTIVATION FOR MULTI-COMPONENT DATA ACQUISITION

In the acoustic forward model, described in paper I, we considered multi-source, multi-receiver reflection measure-
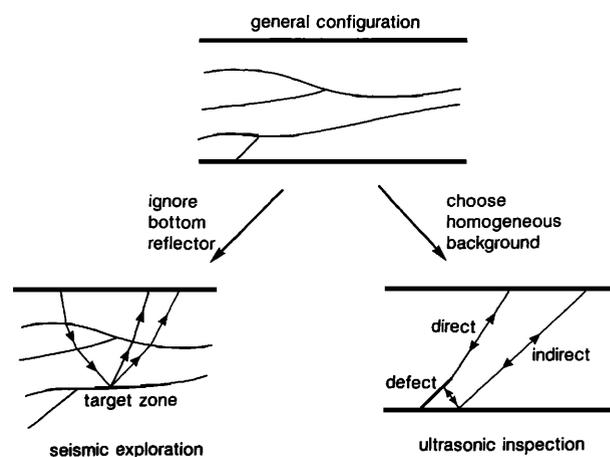

FIG. 1. In this paper the elastic imaging approach is derived for an inhomogeneous bounded solid medium (top figure). For seismic exploration the effects of the lower reflector may be ignored (bottom left); for ultrasonic inspection the background medium may be chosen homogeneous (bottom right).

ments. For each frequency component these measurements were represented by a matrix $\mathbf{P}(z_0)$, in which each element $P_{ij}(z_0)$ represents one Fourier component of an acoustical echo experiment for the ith receiver and the jth source at the acquisition surface z_0. The advantage of carrying out multi-source, multi-receiver experiments is that each subsurface point in the region of interest (target) is illuminated under many angles and that the wave fields scattered by inhomogeneities at any subsurface point are received under many angles. In paper II we made advantageous use of this property by designing an acoustic imaging technique by which the medium inhomogeneities are not only localized but also characterized in terms of their *angle-dependent* reflection properties. In the last step of the full inversion process these angle-dependent reflection properties need to be transformed into the medium parameters of the target (i.e., tissue-oriented, defect-oriented, or litho-oriented parameters in, respectively, medical diagnostics, ultrasonic inspection, and seismic exploration). This last step is in principle possible when only *compressional* (P) wave reflection information is available but the resolution would largely improve when *shear* (S) wave reflection information were also available (de Haas and Berkhout[3]). Therefore each subsurface point in the target should not only be illuminated under different angles but also by different wave types (P and S). Because pure P-wave sources and receivers are never realized in practice (except in fluids, which will not be discussed here), reflection measurements will always contain a mixture of P- and S-wave information. With normal acquisition techniques the P- and S-wave information cannot be well separated and therefore parts of the reflection measurements are erroneously treated by single-wavetype imaging techniques. Therefore, preferably the data acquisition should be carried out with *multi-component* sources and receivers[4] (Fig. 2). The separation of P- and S-wave information should be part of the processing.

II. FORWARD MODEL FOR ELASTIC REFLECTION MEASUREMENTS

In this section we build up the forward model for multi-component elastic reflection measurements step by step. In subsection A we will derive a forward model for the ideal situation, i.e., assuming pure P- and S-wave sources and receivers at a homogeneous (i.e., reflection-free) acquisition surface. In subsection B we will incorporate the effects of the free surface and an optional strong bottom reflector. Finally in subsection C we will transform the pure P- and S-wave responses into realistic responses that would be obtained by multi-component, multi-source, multi-receiver data acquisition. Bear in mind that this forward model is not a proposal for a numerical modeling scheme; it merely serves as a starting point for the stepwise elastic inversion scheme, discussed in the next section.

A. Primary response of pure P- and S-wave sources

Consider the forward model for one Fourier component of discrete *acoustic* primary reflection data (paper I):
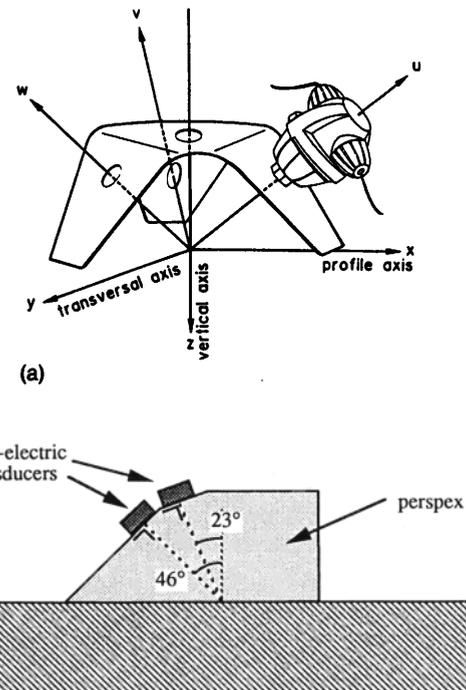

FIG. 2. Multi-component sources and receivers for seismic exploration (a) from Cliet and Dubesset[4] and ultrasonic inspection (b) from M. Lorenz.

$$\mathbf{P}_0^-(z_0) = \mathbf{X}_0^+(z_0, z_0)\mathbf{S}^+(z_0), \qquad (1a)$$

with

$$\mathbf{X}_0^+(z_0, z_0) = \sum_{m=1}^M \mathbf{W}^-(z_0, z_m)\mathbf{R}^+(z_m)\mathbf{W}^+(z_m, z_0). \qquad (1b)$$

In this paper we will use exactly the same formulation for discrete *elastic* primary reflection data. Therefore we redefine the matrices and vectors in Eq. (1). Vector $\mathbf{S}^+(z_0)$ defines a downgoing source wave field at acquisition surface z_0 in terms of independent compressional and shear wave contributions, according to

$$\mathbf{S}^+(z_0) = \begin{bmatrix} \Phi^+(z_0) \\ \Psi_x^+(z_0) \\ \Psi_y^+(z_0) \end{bmatrix}. \qquad (2a)$$

The relation between this downgoing source wave field vector and the actual sources at z_0 is discussed in subsection C of this section.

In a similar way as described in Appendix A of paper I, vector $\Phi^+(z_0)$ contains one frequency component of the discretized version of the downgoing compressional wave potential $\Phi^+(x,y,z_0,\omega)$, whereas vectors $\Psi_x^+(z_0)$ and $\Psi_y^+(z_0)$ contain the discretized versions of the shear wave potentials $\Psi_x^+(x,y,z_0,\omega)$ and $\Psi_y^+(x,y,z_0,\omega)$, respectively (in our notation Ψ_x and Ψ_y represent shear waves polarized perpendicular to the x and the y axis, respectively; shear waves polarized perpendicular to the z axis are not considered separately because they can be obtained by linearly combining Ψ_x and Ψ_y).

In the elastic version of Eq. (1a), vector $\mathbf{P}_0^-(z_0)$ defines

the primary reflected upgoing wave field at acquisition surface z_0, also in terms of independent compressional and shear wave contributions, according to

$$\mathbf{P}_0^-(z_0) = \begin{bmatrix} \mathbf{\Phi}^-(z_0) \\ \mathbf{\Psi}_x^-(z_0) \\ \mathbf{\Psi}_y^-(z_0) \end{bmatrix}_0, \tag{2b}$$

with $\mathbf{\Phi}^-(z_0)$, $\mathbf{\Psi}_x^-(z_0)$, and $\mathbf{\Psi}_y^-(z_0)$ defined in a similar way as above. The relation between this upgoing wave field and the actual measurements at z_0 is discussed in subsection C of this section. (Note that, in analogy with the acoustic situation, the symbols $\mathbf{S}^+$ and $\mathbf{P}_0^-$ denote source wave fields and reflected wave fields; to distinguish between compressional (P) and shear (S) waves we introduced the symbols Φ and Ψ).

Matrix $\mathbf{X}_0^+(z_0,z_0)$ represents the subsurface reflectivity for downgoing waves at z_0, the subscript "0" indicating that surface-related multiple reflections are not yet included. In the elastic situation this matrix consists of nine submatrices, according to

$\mathbf{X}_0^+(z_0,z_0)$

$$= \begin{bmatrix} \mathbf{X}_{\phi,\phi}^+(z_0,z_0) & \mathbf{X}_{\phi,\psi_x}^+(z_0,z_0) & \mathbf{X}_{\phi,\psi_y}^+(z_0,z_0) \\ \mathbf{X}_{\psi_x,\phi}^+(z_0,z_0) & \mathbf{X}_{\psi_x,\psi_x}^+(z_0,z_0) & \mathbf{X}_{\psi_x,\psi_y}^+(z_0,z_0) \\ \mathbf{X}_{\psi_y,\phi}^+(z_0,z_0) & \mathbf{X}_{\psi_y,\psi_x}^+(z_0,z_0) & \mathbf{X}_{\psi_y,\psi_y}^+(z_0,z_0) \end{bmatrix}_0. \tag{3}$$

Any of the submatrices represents the half-space reflectivity for one downgoing source wave type at z_0 and one reflected wave type at z_0.

In Eq. (1b) matrices $\mathbf{W}^+(z_m,z_0)$, $\mathbf{R}^+(z_m)$, and $\mathbf{W}^-(z_0,z_m)$ describe *one-way* downward propagation from z_0 to z_m, reflection at z_m, and upward propagation from z_m to z_0. In the elastic situation these matrices also each contain nine submatrices, according to

$\mathbf{W}^+(z_m,z_0)$

$$= \begin{bmatrix} \mathbf{W}_{\phi,\phi}^+(z_m,z_0) & \mathbf{W}_{\phi,\psi_x}^+(z_m,z_0) & \mathbf{W}_{\phi,\psi_y}^+(z_m,z_0) \\ \mathbf{W}_{\psi_x,\phi}^+(z_m,z_0) & \mathbf{W}_{\psi_x,\psi_x}^+(z_m,z_0) & \mathbf{W}_{\psi_x,\psi_y}^+(z_m,z_0) \\ \mathbf{W}_{\psi_y,\phi}^+(z_m,z_0) & \mathbf{W}_{\psi_y,\psi_x}^+(z_m,z_0) & \mathbf{W}_{\psi_y,\psi_y}^+(z_m,z_0) \end{bmatrix}, \tag{4a}$$

$$\mathbf{R}^+(z_m) = \begin{bmatrix} \mathbf{R}_{\phi,\phi}^+(z_m) & \mathbf{R}_{\phi,\psi_x}^+(z_m) & \mathbf{R}_{\phi,\psi_y}^+(z_m) \\ \mathbf{R}_{\psi_x,\phi}^+(z_m) & \mathbf{R}_{\psi_x,\psi_x}^+(z_m) & \mathbf{R}_{\psi_x,\psi_y}^+(z_m) \\ \mathbf{R}_{\psi_y,\phi}^+(z_m) & \mathbf{R}_{\psi_y,\psi_x}^+(z_m) & \mathbf{R}_{\psi_y,\psi_y}^+(z_m) \end{bmatrix} \tag{4b}$$

(see the Appendix), and

$\mathbf{W}^-(z_0,z_m)$

$$= \begin{bmatrix} \mathbf{W}_{\phi,\phi}^-(z_0,z_m) & \mathbf{W}_{\phi,\psi_x}^-(z_0,z_m) & \mathbf{W}_{\phi,\psi_y}^-(z_0,z_m) \\ \mathbf{W}_{\psi_x,\phi}^-(z_0,z_m) & \mathbf{W}_{\psi_x,\psi_x}^-(z_0,z_m) & \mathbf{W}_{\psi_x,\psi_y}^-(z_0,z_m) \\ \mathbf{W}_{\psi_y,\phi}^-(z_0,z_m) & \mathbf{W}_{\psi_y,\psi_x}^-(z_0,z_m) & \mathbf{W}_{\psi_y,\psi_y}^-(z_0,z_m) \end{bmatrix}. \tag{4c}$$

Each submatrix is defined in a similar way as in the acoustic situation (paper I, Appendixes B and C). For example, submatrix $\mathbf{W}_{\psi_y,\phi}^+(z_m,z_0)$ describes the downward propagation

from P waves at z_0, i.e., vector $\mathbf{\Phi}^+(z_0)$, to S_y waves at z_m, i.e., vector $\mathbf{\Psi}_y^+(z_m)$. Hence, each column of this submatrix equals (one Fourier component of) the S_y-wave response at depth level z_m due to one P-wave dipole source at the surface z_0 (Wapenaar and Berkhout,[5] Chap. VI).

Similarly, submatrix $\mathbf{R}_{\psi_y,\phi}^+(z_m)$ describes the (angle-dependent) reflection from downgoing P waves at z_m, i.e., vector $\mathbf{\Phi}^+(z_m)$, to upgoing S_y waves at z_m, i.e., vector $\mathbf{\Psi}_y^-(z_m)$. Hence, each column of this submatrix equals (one Fourier component of) the reflected S_y-wave response at depth level z_m due to one P-wave dipole source at depth level z_m.

In summary, the forward model of Eq. (1) describes the response of the *inhomogeneous* elastic medium ($z_0 < z \leqslant z_M$) in terms of the primary reflected upgoing P and S waves at z_0 due to downgoing P and S waves at z_0. The situation is schematically visualized in Fig. 3.

B. Incorporation of multiple reflections

In paper I we generalized the acoustic version of our forward model as to include surface related as well as *internal* multiple reflections. Of course the same procedure could be followed for the elastic situation but this will not be repeated here.

As explained in the introduction we will consider a perfectly reflecting acquisition surface z_0 as well as a strong reflector at z_M; in the region between z_0 and z_M we will assume low contrasts. The reflecting surface at z_0 will give rise to surface-related multiple reflections in a similar manner as explained in paper I; the strong reflector at z_M will give rise to bottom related multiple reflections.

Let us start with the surface-related multiple reflections, by modifying Eq. (1a) to

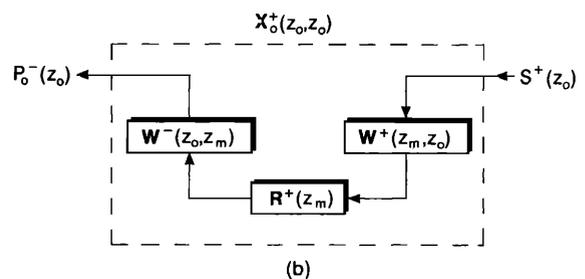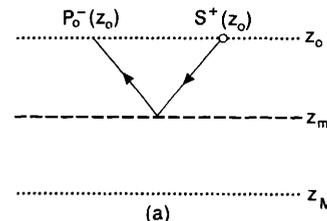$$\mathbf{P}^-(z_0) = \mathbf{X}_0^+(z_0,z_0)\mathbf{P}^+(z_0), \tag{5a}$$

FIG. 3. Forward model for the primary upgoing response of an elastic medium due to a downgoing source wave field at z_0. (a) Simplified configuration with one reflecting interface at z_m. The "rays" symbolically represent elastic wave fields (P and S waves). Dashed lines denote a low contrast, dotted lines denote a reference depth level without contrast. (b) Block diagram.

where the downgoing wave field $P^+(z_0)$ consists of the downgoing source wave field $S^+(z_0)$, increased with the downwardly reflected upgoing waves at z_0, hence

$$P^+(z_0) = S^+(z_0) + R^-(z_0)P^-(z_0), \quad (5b)$$

see Fig. 4. An expression for the free-surface reflection matrix $R^-(z_0)$ is derived in subsection C of this section. Substituting (5b) into (5a) and rewriting the expression in a similar form as (1a) yields

$$P^-(z_0) = X^+(z_0,z_0)S^+(z_0), \quad (6a)$$

where

$$X^+(z_0,z_0) = [I - X_0^+(z_0,z_0)R^-(z_0)]^{-1}X_0^+(z_0,z_0). \quad (6b)$$

Next we discuss the effect of the bottom reflector at z_M. Bear in mind that this reflector acts as a mirror for the sources and receivers at z_0. Therefore we first derive a forward model for *virtual* sources and receivers at z_M.

The relation between the virtual source and its response at z_M reads, in analogy with Eqs. (1a) and (1b),

$$P_0^+(z_M) = X_0^-(z_M,z_M)S^-(z_M), \quad (7a)$$

with

$$X_0^-(z_M,z_M) = \sum_{m=1}^{M-1} W^+(z_M,z_m)R^-(z_m)W^-(z_m,z_M), \quad (7b)$$

see Fig. 5.

Taking bottom-related multiple reflections into account yields, in analogy with Eqs. (6a) and (6b),

$$P^+(z_M) = X^-(z_M,z_M)S^-(z_M), \quad (8a)$$

where

$$X^-(z_M,z_M) = [I - X_0^-(z_M,z_M)R^+(z_M)]^{-1}X_0^-(z_M,z_M), \quad (8b)$$

FIG. 5. Forward model for the primary downgoing response of an elastic medium due to a virtual upgoing source wave field at z_M. (a) Simplified configuration with one reflecting interface at z_m. (b) Block diagram.

see Fig. 6. The virtual source wave field $S^-(z_M)$ is related to the actual downgoing source wave field $S^+(z_0)$ according to

$$S^-(z_M) = R^+(z_M)W^+(z_M,z_0)S^+(z_0). \quad (9)$$

Similarly, the relation between the virtual source response $P^+(z_M)$ and the received upgoing wave field at the surface reads

$$P_v^-(z_0) = W^-(z_0,z_M)R^+(z_M)P^+(z_M), \quad (10)$$

index "v" denoting "virtual."

The combination of Eqs. (8), (9), and (10) yields

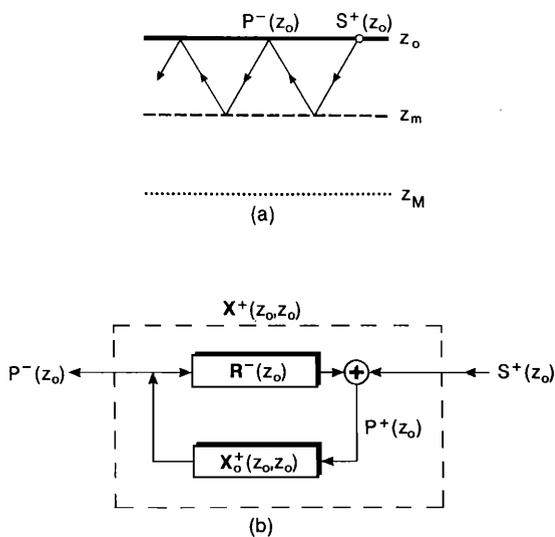$$P_v^-(z_0) = X_v^+(z_0,z_0)S^+(z_0), \quad (11a)$$

where

FIG. 4. As in Fig. 3, including surface-related multiple reflections. (a) Simplified configuration (the heavy line denotes the free surface). (b) Block diagram.
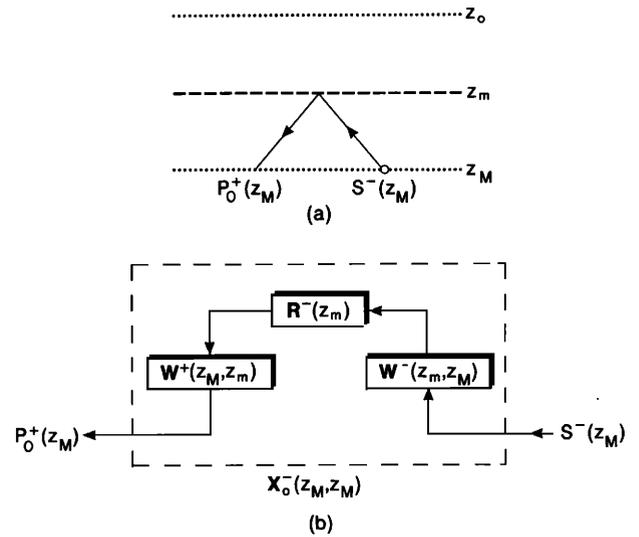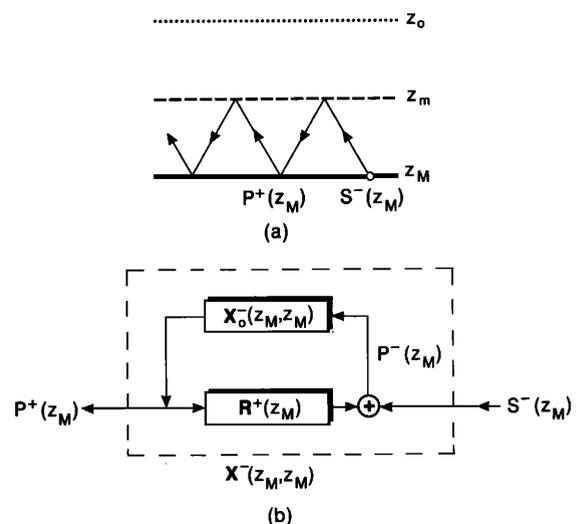

FIG. 6. As in Fig. 5, including bottom related reflections. (a) Simplified configuration (the heavy solid line denotes the bottom reflector). (b) Block diagram.

$$\mathbf{X}_v^+(z_0,z_0) = \mathbf{W}^-(z_0,z_M)[\mathbf{R}^+(z_M)\mathbf{X}^-(z_M,z_M)\mathbf{R}^+(z_M)]$$
$$\times\mathbf{W}^+(z_M,z_0), \qquad (11b)$$

see Fig. 7.

This virtual source response ("indirect response," see also Fig. 1) should be added to the original *primary* response ("direct response"), hence, Eq. (1) should be modified to

$$\mathbf{P}_{0,v}^-(z_0) = \mathbf{X}_{0,v}^+(z_0,z_0)\mathbf{S}^+(z_0), \qquad (12a)$$

where

$$\mathbf{X}_{0,v}^+(z_0,z_0) = \mathbf{X}_0^+(z_0,z_0) + \mathbf{X}_v^+(z_0,z_0), \qquad (12b)$$

see Fig. 8. Consequently, Eq. (6) should be modified to

$$\mathbf{P}^-(z_0) = \mathbf{X}^+(z_0,z_0)\mathbf{S}^+(z_0), \qquad (13a)$$

where

$$\mathbf{X}^+(z_0,z_0) = [\mathbf{I} - \mathbf{X}_{0,v}^+(z_0,z_0)\mathbf{R}^-(z_0)]^{-1}\mathbf{X}_{0,v}^+(z_0,z_0), \qquad (13b)$$

see Fig. 9. Summarizing the aforegoing, we may write for $\mathbf{X}_{0,v}^+(z_0,z_0)$:

$$\mathbf{X}_{0,v}^+(z_0,z_0)$$
$$= \sum_{m=1}^{M} \mathbf{W}^-(z_0,z_m)\mathbf{R}^+(z_m)\mathbf{W}^+(z_m,z_0)$$
$$+ \mathbf{W}^-(z_0,z_M)[\mathbf{R}^+(z_M)\mathbf{X}^-(z_M,z_M)\mathbf{R}^+(z_M)]$$
$$\mathbf{W}^+(z_M,z_0), \qquad (13c)$$

where

$$\mathbf{X}^-(z_M,z_M)$$
$$= [\mathbf{I} - \mathbf{X}_0^-(z_M,z_M)\mathbf{R}^+(z_M)]^{-1}\mathbf{X}_0^-(z_M,z_M) \qquad (13d)$$

with

$$\mathbf{X}_0^-(z_M,z_M) = \sum_{m=1}^{M-1} \mathbf{W}^+(z_M,z_m)\mathbf{R}^-(z_m)\mathbf{W}^-(z_m,z_M). \qquad (13e)$$
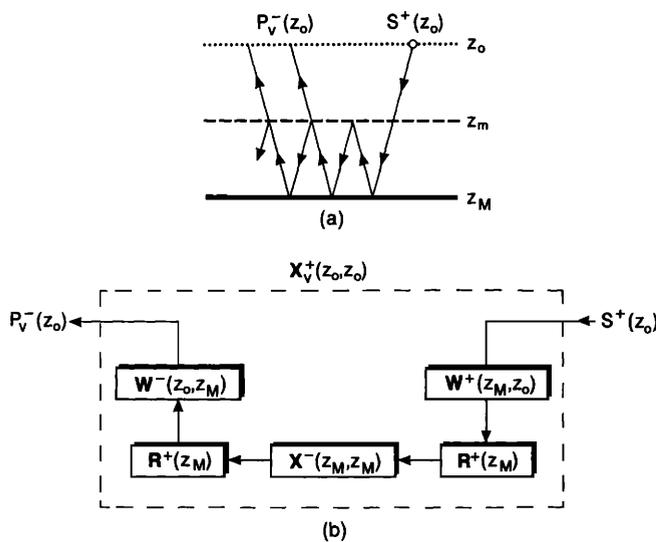
The forward model of Eq. (13) describes the response of

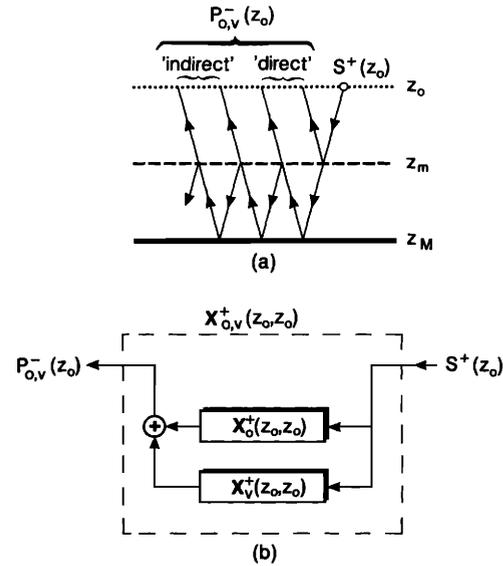FIG. 7. Forward model for the virtual source response ("indirect illumination") at z_0.

FIG. 8. Superposition of the "direct" (Fig. 3) and "indirect" (Fig. 7) responses.

the inhomogeneous elastic medium $(z_0 \leqslant z \leqslant z_M)$ in terms of the upgoing P and S waves at z_0 due to downgoing P and S waves at z_0. Multiple reflections related to the free surface z_0 and the bottom reflector at z_M are included. Internal multiples have been neglected.

C. Incorporation of sources and receivers

The downgoing source wave field $\mathbf{S}^+(z_0)$ and the upgoing reflected wave field $\mathbf{P}^-(z_0)$ in Eq. (13a) are *one-way* wave fields. In this section we derive the relation between these one-way wave fields and the actual sources and received wave fields at z_0. First, consider the general relationship between elastic *two-way* and *one-way* wave fields at depth level z (see the Appendix):

$$\begin{bmatrix} \mathbf{V}(z) \\ \mathbf{T}(z) \end{bmatrix} = \begin{bmatrix} \mathbf{L}_1^+(z) & \mathbf{L}_1^-(z) \\ \mathbf{L}_2^+(z) & \mathbf{L}_2^-(z) \end{bmatrix} \begin{bmatrix} \mathbf{P}^+(z) \\ \mathbf{P}^-(z) \end{bmatrix}, \qquad (14a)$$
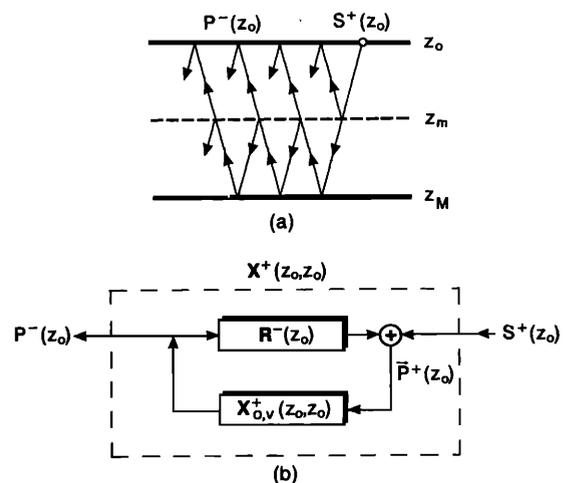

FIG. 9. As in Fig. 8, including surface-related multiple reflections.

where the *three-component* velocity and traction vectors $V(z)$ and $T(z)$ are defined according to

$$V(z) = \begin{bmatrix} V_x(z) \\ V_y(z) \\ V_z(z) \end{bmatrix} \qquad (14b)$$

and

$$T(z) = \begin{bmatrix} T_x(z) \\ T_y(z) \\ T_z(z) \end{bmatrix}. \qquad (14c)$$

In (14b), vectors $V_x(z)$, $V_y(z)$, and $V_z(z)$ contain one Fourier component of the discretized versions of the particle velocity components $V_x(x,y,z,\omega)$, $V_y(x,y,z,\omega)$, and $V_z(x,y,z,\omega)$, respectively, at depth level z. Similarly, in (14c) vectors $T_x(z)$, $T_y(z)$, and $T_z(z)$ contain the traction components $T_x(x,y,z,\omega)$, $T_y(x,y,z,\omega)$, and $T_z(x,y,z,\omega)$, respectively, also at depth level z.

In the following we restrict ourselves for simplicity to the situation where the sources and receivers are *at* the free surface. Upon substitution of Eq. (5b) into (14a) we obtain the following two equations for the particle velocity and traction, respectively, at the free surface:

$$V(z_0) = L_1^+(z_0)S^+(z_0)$$
$$+ [L_1^+(z_0)R^-(z_0) + L_1^-(z_0)]P^-(z_0) \qquad (15a)$$

and

$$T(z_0) = L_2^+(z_0)S^+(z_0)$$
$$+ [L_2^+(z_0)R^-(z_0) + L_2^-(z_0)]P^-(z_0). \qquad (15b)$$

The traction at the free surface must be zero, except at the sources. In other words, $T(z_0)$ in (15b) is by definition the source traction and the only contribution comes from $S^+(z_0)$, hence

$$T(z_0) = L_2^+(z_0)S^+(z_0) \qquad (16a)$$

and

$$[L_2^+(z_0)R^-(z_0) + L_2^-(z_0)]P^-(z_0) = 0. \qquad (16b)$$

Hence, if we define the *source-decomposition* process as

$$S^+(z_0) \triangleq D^+(z_0)T(z_0), \qquad (17a)$$

then from Eq. (16a) we easily obtain the following expression for the source–decomposition operator:

$$D^+(z_0) = (L_2^+(z_0))^{-1}. \qquad (17b)$$

Furthermore, since Eq. (16b) should hold for any upgoing wave field $P^-(z_0)$, we obtain for the free-surface reflection operator

$$R^-(z_0) = -(L_2^+(z_0))^{-1}L_2^-(z_0). \qquad (17c)$$

Substitution of these results in (15a) yields for the particle velocity at the free surface

$$V(z_0) = V_s(z_0) + V_r(z_0), \qquad (18a)$$

where the direct source wave contribution $V_s(z_0)$ reads

$$V_s(z_0) = L_1^+(z_0)(L_2^+(z_0))^{-1}T(z_0) \qquad (18b)$$

and where the reflected wave contribution $V_r(z_0)$ reads

$$V_r(z_0) = [-L_1^+(z_0)(L_2^+(z_0))^{-1}L_2^-(z_0) + L_1^-(z_0)]$$
$$\times P^-(z_0), \qquad (18c)$$

or, according to Eq. (A1c),

$$V_r(z_0) = (N_1^-(z_0))^{-1}P^-(z_0). \qquad (18d)$$

When the shallow subsurface contains no significant contrasts, then $V_s(z_0)$ contains only surface wave information (nondispersed Rayleigh waves) whereas $V_r(z_0)$ contains only body wave information (i.e., the reflections of the subsurface). On the other hand, when significant contrasts are present in the shallow subsurface, then the *dispersed* Rayleigh-wave and Love-wave information will be distributed over $V_s(z_0)$ and $V_r(z_0)$. In the following, the latter situation will be discarded for simplicity. Hence, we will assume that the surface waves are described exclusively by Eq. (18b):

$$V_s(z_0) = Y_s(z_0,z_0)T(z_0), \qquad (19a)$$

where the *surface wave admittance* operator $Y_s(z_0,z_0)$ is defined as

$$Y_s(z_0,z_0) = L_1^+(z_0)(L_2^+(z_0))^{-1}. \qquad (19b)$$

As a consequence, the subsurface reflections are described exclusively by Eq. (18d):

$$V_r(z_0) = D^-(z_0)P^-(z_0), \qquad (20a)$$

where the *receiver–composition* operator is defined as

$$D^-(z_0) = (N_1^-(z_0))^{-1}. \qquad (20b)$$

Note that the forward model of Eq. (13a) may be elegantly combined with the decomposition and composition equations (17a) and (20a), respectively, yielding

$$V_r(z_0) = D^-(z_0)X^+(z_0,z_0)D^+(z_0)T(z_0), \qquad (21)$$

see Fig. 10. From right to left, Eq. (21) contains a source vector (describing the traction distribution imposed by a source at the free surface), a decomposition operator (transforming the traction into downgoing P and S waves), a subsurface reflectivity operator (describing the response of the subsurface, including multiple reflections related to the free surface and, optionally, the bottom reflector), and a composition operator (transforming the upgoing P and S waves into particle velocities at the free surface). Note that, in analogy with Eq. (19a), Eq. (21) may be rewritten as

$$V_r(z_0) = Y_r(z_0,z_0)T(z_0), \qquad (22a)$$

where the *body wave admittance* operator $Y_r(z_0,z_0)$ is defined as

$$Y_r(z_0,z_0) = D^-(z_0)X^+(z_0,z_0)D^+(z_0). \qquad (22b)$$
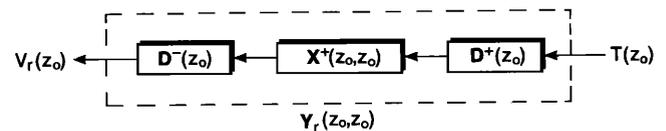
Similarly, for the total response we may write

FIG. 10. Forward model describing the relation between the subsurface response matrix $X^+(z_0,z_0)$ and the sources and receivers at the free surface.

$$V(z_0) = Y(z_0,z_0)T(z_0), \qquad (23a)$$

where

$$Y(z_0,z_0) = Y_s(z_0,z_0) + Y_r(z_0,z_0), \qquad (23b)$$

see Fig. 11. Equation (23), with $Y_s(z_0,z_0)$ and $Y_r(z_0,z_0)$ defined by Eqs. (19b) and (22b), respectively, is the forward model for one frequency component of *one* multi-component echo experiment.

In accordance with Eq. (14b), vector $V(z_0)$ contains the particle velocity components measured at the free surface. In accordance with Eq. (14c), vector $T(z_0)$ contains the source traction vectors $T_x(z_0)$, $T_y(z_0)$, and $T_z(z_0)$. For a point source of tensile stress, vectors $T_x(z_0)$ and $T_y(z_0)$ are zero whereas vector $T_z(z_0)$ contains only one nonzero element, its value representing the source signature $S(\omega)$ for the frequency component of interest. Similarly, for a point source of shearing stress one of the vectors $T_x(z_0)$ or $T_y(z_0)$ contains only one nonzero element, its value again representing $S(\omega)$. When the source is not an ideal point source then the source vectors contain the stress *distribution* at z_0. The forward model for one reflection experiment can be easily extended to a forward model for the multi-experiment situation. Ideally, three independent experiments should be carried out for each source position by applying three differently oriented stresses. For the 3×3 component multi-experiment situation the extended forward model reads

$$V(z_0) = Y(z_0,z_0)T(z_0). \qquad (24)$$

Here the columns of the data matrix $V(z_0)$ contain the different data vectors $V(z_0)$. The columns of the source matrix $T(z_0)$ contain the corresponding source vectors $T(z_0)$. When use is made of mutually perpendicular sources then the source vectors can be ordered in such a way that the source matrix can be written as

$$T(z_0) = \begin{bmatrix} T_x(z_0) & 0 & 0 \\ 0 & T_y(z_0) & 0 \\ 0 & 0 & T_z(z_0) \end{bmatrix}. \qquad (25a)$$

Moreover, for identical point sources this expression may be further simplified to

$$T(z_0) = S(\omega)I. \qquad (25b)$$

Now matrix $V(z_0)$ in Eq. (24) may be written as

$$V(z_0) = \begin{bmatrix} V_{x,x}(z_0) & V_{x,y}(z_0) & V_{x,z}(z_0) \\ V_{y,x}(z_0) & V_{y,y}(z_0) & V_{y,z}(z_0) \\ V_{z,x}(z_0) & V_{z,y}(z_0) & V_{z,z}(z_0) \end{bmatrix}, \qquad (26)$$
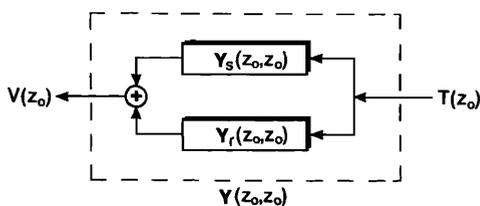

FIG. 11. The measured particle velocity at the free surface as a superposition of surface waves and body waves.

where any of the submatrices $V_{i,j}(z_0)$ for $i = x,y,z$ and $j = x,y,z$ represents a single-component dataset for which the acquisition is carried out with velocity receivers oriented in the i direction and stress sources oriented in the j direction.

In practice, however, the receivers and sources do not act in mutually perpendicular directions, see Fig. 2. To obtain the multi-component dataset measured with the actual receivers and sources the data matrix $V(z_0)$, as defined in Eq. (26), should be pre- and post-multiplied by matrices containing the direction cosines of the dip and azimuth angles of the velocity receivers and stress sources, respectively. A further discussion of this trivial procedure is beyond the scope of this paper.

III. ELASTIC INVERSION IN STEPS

In paper II we have approached the acoustic imaging problem from different angles, finally leading to the conclusion that in the most general situation imaging may be seen as one step of a full inversion proces. In this section we will elaborate on this concept and discuss the extension to the full elastic situation.

In Sec. II we derived a forward model for elastic reflection measurements. This forward model was built up step by step by applying a number of matrix manipulations to the subsurface reflectivity matrices. The stepwise elastic inversion scheme will now be derived by applying the same matrix manipulations in reverse order. In subsection A of this section we discuss surface related pre-processing; i.e., decomposition of the measurements into downgoing and upgoing P and S waves at the surface and elimination of the surface related multiple reflections. In subsection B of this section we discuss the elimination of propagation effects (redatuming), resulting in an image of the subsurface reflectivity. In subsection C of this section we briefly discuss some aspects of target related model fitting, yielding a quantitative description of the target. Bear in mind that the proposed elastic inversion scheme is based on the assumption that multi-component, multi-source, multi-receiver data are available. Due to the limitations of data acquisition in practice, often a simplified version of the elastic inversion scheme must be employed.

A. Surface related pre-processing

When the receivers and sources are oriented in arbitrary directions (Fig. 2), mutually perpendicular receivers and sources should be simulated first by applying a weighted summation to the different responses, the weighting factors being determined by the direction cosines of the dip and azimuth angles of the velocity receivers and stress sources. Next, a Fourier transform (from time to frequency) should be applied to each recorded signal, thus decomposing the data into monochromatic datasets $V(z_0)$ [Eq. (26)]. Any of these monochromatic datasets satisfy the forward model described in Sec. II. According to Eq. (24), with $Y(z_0,z_0)$ and $T(z_0)$ defined by (23b) and (25b), respectively, we may write for one frequency component of the measured data

$$V(z_0) = [Y_s(z_0,z_0) + Y_r(z_0,z_0)]S(\omega) \qquad (27)$$

(see also Fig. 11), where $S(\omega)$ represents one frequency component of the source signature and where $\mathbf{Y}_s(z_0,z_0)$ and $\mathbf{Y}_r(z_0,z_0)$, respectively, represent the surface and body wave admittance operators. The surface wave admittance operator $\mathbf{Y}_s(z_0,z_0)$ is determined by the propagation properties of the medium directly below the free surface z_0. Hence, the surface wave information contained in the data matrix $\mathbf{V}(z_0)$ can be used to estimate simultaneously the near surface propagation properties and the source signature $\widehat{S}(\omega)$. The Rayleigh wave *traveltime* information is used to construct an initial model. This initial model as well as the initial source signature are updated via an optimization algorithm by matching the simulated surface waves with the actually measured surface waves ("data fitting"). Once the mismatch is acceptable, the modeled surface waves are subtracted from the measured data, according to

$$\widehat{\mathbf{V}}_r(z_0) = \mathbf{V}(z_0) - \widehat{\mathbf{Y}}_s(z_0,z_0)\widehat{S}(\omega), \qquad (28a)$$

where $\widehat{\mathbf{V}}_r(z_0)$ represents an estimate of the subsurface reflections $\mathbf{V}_r(z_0)$, defined as

$$\mathbf{V}_r(z_0) = \mathbf{Y}_r(z_0,z_0)S(\omega), \qquad (28b)$$

or

$$\mathbf{V}_r(z_0) = \mathbf{D}^-(z_0)\mathbf{X}^+(z_0,z_0)\mathbf{D}^+(z_0)S(\omega), \qquad (28c)$$

see also Eq. (22) and Fig. 10. We are now ready to derive the decomposition algorithm. Remember that matrix $\mathbf{X}^+(z_0,z_0)$ in Eq. (28c) describes the subsurface response in terms of the upgoing P and S waves at z_0 due to downgoing P and S waves at z_0. Hence, decomposition into downgoing and upgoing P and S waves is accomplished by inverting equation (28c), according to Wapenaar *et al.*[6]

$$\widehat{\mathbf{P}}^-(z_0) = [\widehat{\mathbf{D}}^-(z_0)]^{-1}\widehat{\mathbf{V}}_r(z_0)[\widehat{\mathbf{D}}^+(z_0)]^{-1}, \qquad (29a)$$

where $\widehat{\mathbf{P}}^-(z_0)$ represents an estimate of the upgoing wave field matrix $\mathbf{P}^-(z_0)$, defined as

$$\mathbf{P}^-(z_0) = \mathbf{X}^+(z_0,z_0)S(\omega) \qquad (29b)$$

and where

$$[\widehat{\mathbf{D}}^+(z_0)]^{-1} = \widehat{\mathbf{L}}_2^+(z_0) \qquad (29c)$$

and

$$[\widehat{\mathbf{D}}^-(z_0)]^{-1} = \widehat{\mathbf{N}}_1^-(z_0), \qquad (29d)$$

see Eqs. (17b) and (20b), respectively. Note the similarity of Eq. (29a) with "image formation by double inversion," see Fig. 1 in paper II. According to (29a) decomposition involves application of the matrix operators $[\widehat{\mathbf{D}}^-(z_0)]^{-1}$ and $[\widehat{\mathbf{D}}^+(z_0)]^{-1}$ to the data matrix $\widehat{\mathbf{V}}_r(z_0)$. Note that $[\widehat{\mathbf{D}}^-(z_0)]^{-1}\widehat{\mathbf{V}}_r(z_0)$ describes a generalized lateral deconvolution process along the columns (i.e., the monochromatic common source experiments) of matrix $\widehat{\mathbf{V}}_r(z_0)$. This operation accounts for the decomposition of the received wave fields into upgoing P and S waves. Similarly, $\widehat{\mathbf{V}}_r(z_0)[\widehat{\mathbf{D}}^+(z_0)]^{-1}$ describes a generalized lateral deconvolution process along the rows (i.e., the monochromatic common receiver experiments) of matrix $\widehat{\mathbf{V}}_r(z_0)$. This operation accounts for the decomposition of the emitted wave fields into downgoing P and S waves. Note that decomposition, as described by Eq. (29a), fully accounts for lateral

variations of the near surface propagation properties.

In Eqs. (29c) and (29d), matrices $\widehat{\mathbf{L}}_2^+(z_0)$ and $\widehat{\mathbf{N}}_1^-(z_0)$ are obtained by substituting the previously estimated near surface propagation properties into the expressions for $\mathbf{L}_2^+(z_0)$ and $\mathbf{N}_1^-(z_0)$, respectively. Note that the estimated near-surface propagation properties may be further improved by minimizing the total entropy (i.e., disorder, Smith and Grandy[7]) in the decomposed (i.e., ordered) datasets $\widehat{\mathbf{P}}^-(z_0)$ for all frequency components of interest.

Next we derive the algorithm for surface-related multiple elimination. As mentioned above, the decomposed dataset $\widehat{\mathbf{P}}^-(z_0)$ represents an estimate of the upgoing wave field matrix $\mathbf{P}^-(z_0)$, defined by

$$\mathbf{P}^-(z_0) = \mathbf{X}^+(z_0,z_0)S(\omega), \qquad (30a)$$

where, according to (13b),

$$\mathbf{X}^+(z_0,z_0) = [\mathbf{I} - \mathbf{X}_{0,v}^+(z_0,z_0)\mathbf{R}^-(z_0)]^{-1}\mathbf{X}_{0,v}^+(z_0,z_0), \qquad (30b)$$

see also Fig. 9. Remember that $\mathbf{X}_{0,v}^+(z_0,z_0)$ describes the subsurface response without surface related multiples. Hence, surface related multiple elimination is accomplished by inverting Eqs. (30a) and (30b) according to

$$\widehat{\mathbf{X}}^+(z_0,z_0) = \widehat{\mathbf{P}}^-(z_0)[\widehat{S}(\omega)]^{-1} \qquad (31a)$$

(deconvolution), followed by

$$\widehat{\mathbf{X}}_{0,v}^+(z_0,z_0) = \widehat{\mathbf{X}}^+(z_0,z_0)[\mathbf{I} + \widehat{\mathbf{R}}^-(z_0)\widehat{\mathbf{X}}^+(z_0,z_0)]^{-1}. \qquad (31b)$$

In (31a) $\widehat{S}(\omega)$ is the previously estimated source signature; in (31b) $\widehat{\mathbf{R}}^-(z_0)$ is obtained by substituting the previously estimated near surface propagation properties into the expression for $\mathbf{R}^-(z_0)$. Note that the estimated source signature as well as the near-surface propagation properties may be further improved by minimizing the total energy in the "multiple free" response matrices $\widehat{\mathbf{X}}_{0,v}^+(z_0,z_0)$ for all frequency components of interest (Verschuur *et al.*[8]).

In summary, for the full elastic situation, surface-related pre-processing involves elimination of the surface waves according to Eq. (28a), decomposition into one-way P and S waves according to Eq. (29a), deconvolution according to Eq. (31a), and multiple elimination according to Eq. (31b).

Note that no prior information about the subsurface is required. Apart from the data $\mathbf{V}(z_0)$, the only extra information needed are the source signature and the near-surface propagation properties. These are estimated along with the surface-wave elimination and are further improved during decomposition and multiple elimination.

B. Redatuming and imaging

The output of surface related pre-processing, matrix $\widehat{\mathbf{X}}_{0,v}^+(z_0,z_0)$, represents an estimate of the subsurface response matrix $\mathbf{X}_{0,v}^+(z_0,z_0)$, defined as

$$\mathbf{X}_{0,v}^+(z_0,z_0) = \mathbf{X}_0^+(z_0,z_0) + \mathbf{X}_v^+(z_0,z_0), \qquad (32a)$$

see Fig. 8, where $\mathbf{X}_0^+(z_0,z_0)$ represents the subsurface response for "direct illumination," according to

$$X_0^+ (z_0,z_0) = \sum_{m=1}^{M} W^- (z_0,z_m) R^+ (z_m) W^+ (z_m,z_0),$$

$$(32b)$$

see Fig. 3, and where $X_v^+ (z_0,z_0)$ represents the subsurface response for "indirect illumination" via a strong bottom reflector at z_M, according to

$$X_v^+ (z_0,z_0) = W^- (z_0,z_M) [R^+ (z_M) X^- (z_M,z_M) R^+ (z_M)]$$

$$\times W^+ (z_M,z_0), \quad (32c)$$

see Fig. 7. For the moment we only consider the subsurface response for direct illumination. Note that $X_0^+ (z_0,z_0)$ is a distorted version of the subsurface reflection matrices $R^+ (z_m)$, the distortions being determined by the propagation matrices $W^+ (z_m,z_0)$ and $W^- (z_0,z_m)$. Hence, reflection imaging involves elimination of the propagation distortions, i.e., inversion of the propagation matrices, according to

$$W^+ (z_m,z_0) F^+ (z_0,z_m) = I \quad (33a)$$

and

$$F^- (z_m,z_0) W^- (z_0,z_m) = I. \quad (33b)$$

In practice these results can never be reached. In analogy with the acoustic situation we define stable spatially bandlimited versions of the inverse matrices as

$$\hat{F}^+ (z_0,z_m) = [\hat{W}^- (z_0,z_m)]^* \quad (34a)$$

and

$$\hat{F}^- (z_m,z_0) = [\hat{W}^+ (z_m,z_0)]^* \quad (34b)$$

(Wapenaar and Berkhout,[5] 1989, Chap. VIII), where $\hat{W}^+$ and $\hat{W}^-$ are based on an estimated macro model of the subsurface. A discussion on macro model estimation is beyond the scope of this paper. (For ultrasonic inspection the macro model may often be taken homogeneous; for seismic exploration we refer to the proceedings of the EAEG workshop on macro model estimation.[9])

Applying $\hat{F}^+$ and $\hat{F}^-$ to the subsurface response matrix $\hat{X}_0^+$ yields

$$\hat{X}_0^+ (z_m,z_m) = \hat{F}^- (z_m,z_0) \hat{X}_0^+ (z_0,z_0) \hat{F}^+ (z_0,z_m). \quad (35)$$

Note that the so-called *redatumed* subsurface response at z_m, matrix $\hat{X}_0^+ (z_m,z_m)$, contains a spatially bandlimited version of the reflection matrix $R^+ (z_m)$ and propagation distorted contributions from matrices $R^+ (z_k)$ for all $k \neq m$. The latter can be suppressed by averaging over all available frequency components ω_n, according to

$$\hat{R}^+ (z_m) = \frac{1}{N} \sum_n \hat{X}_0^+ (z_m,z_m), \quad (36)$$

where N is the number of frequency components.

This process is called *imaging*. In paper II we discussed a generalization imaging procedure, based on Radon transforms, which preserves the *angle-dependent* properties of the reflection matrix. This generalized imaging procedure, which can also be applied to any of the nine submatrices in $\hat{X}_0^+ (z_m,z_m)$, will not be repeated here.

Consider again Eq. (35), which describes redatuming of the subsurface response from the surface z_0 to depth z_m. Similar as matrices W^+ and W^- [Eq. (4)], the inverse matri-

ces $\hat{F}^+$ and $\hat{F}^-$ in Eq. (35) each contain nine submatrices, according to

$$\hat{F}^+ (z_0,z_m)$$

$$= \begin{bmatrix} \hat{F}_{\phi,\phi}^+ (z_0,z_m) & \hat{F}_{\phi,\psi_x}^+ (z_0,z_m) & \hat{F}_{\phi,\psi_y}^+ (z_0,z_m) \\ \hat{F}_{\psi_x,\phi}^+ (z_0,z_m) & \hat{F}_{\psi_x,\psi_x}^+ (z_0,z_m) & \hat{F}_{\psi_x,\psi_y}^+ (z_0,z_m) \\ \hat{F}_{\psi_y,\phi}^+ (z_0,z_m) & \hat{F}_{\psi_y,\psi_x}^+ (z_0,z_m) & \hat{F}_{\psi_y,\psi_y}^+ (z_0,z_m) \end{bmatrix}$$

$$(37a)$$

and

$$\hat{F}^- (z_m,z_0)$$

$$= \begin{bmatrix} \hat{F}_{\phi,\phi}^- (z_m,z_0) & \hat{F}_{\phi,\psi_x}^- (z_m,z_0) & \hat{F}_{\phi,\psi_y}^- (z_m,z_0) \\ \hat{F}_{\psi_x,\phi}^- (z_m,z_0) & \hat{F}_{\psi_x,\psi_x}^- (z_m,z_0) & \hat{F}_{\psi_x,\psi_y}^- (z_m,z_0) \\ \hat{F}_{\psi_y,\phi}^- (z_m,z_0) & \hat{F}_{\psi_y,\psi_x}^- (z_m,z_0) & \hat{F}_{\psi_y,\psi_y}^- (z_m,z_0) \end{bmatrix}.$$

$$(37b)$$

When wave conversion *during propagation* is neglected, these matrices may be simplified to

$$\hat{F}^+ (z_0,z_m)$$

$$= \begin{bmatrix} \hat{F}_{\phi,\phi}^+ (z_0,z_m) & 0 & 0 \\ 0 & \hat{F}_{\psi_x,\psi_x}^+ (z_0,z_m) & 0 \\ 0 & 0 & \hat{F}_{\psi_y,\psi_y}^+ (z_0,z_m) \end{bmatrix},$$

$$(38a)$$

and

$$\hat{F}^- (z_m,z_0)$$

$$= \begin{bmatrix} \hat{F}_{\phi,\phi}^- (z_m,z_0) & 0 & 0 \\ 0 & \hat{F}_{\psi_x,\psi_x}^- (z_m,z_0) & 0 \\ 0 & 0 & \hat{F}_{\psi_y,\psi_y}^- (z_m,z_0) \end{bmatrix},$$

$$(38b)$$

respectively. With these definitions, Eq. (35) can be rewritten into nine *independent* redatuming equations for the submatrices in $\hat{X}_0^+ (z_0,z_0)$. We give three examples:

$$\hat{X}_{\phi,\phi}^+ (z_m,z_m) = \hat{F}_{\phi,\phi}^- (z_m,z_0) X_{\phi,\phi}^+ (z_0,z_0) \hat{F}_{\phi,\phi}^+ (z_0,z_m), \quad (39a)$$

$$\hat{X}_{\psi_y,\psi_y}^+ (z_m,z_m) = \hat{F}_{\psi_y,\psi_y}^- (z_m,z_0) X_{\psi_y,\psi_y}^+ (z_0,z_0) \hat{F}_{\psi_y,\psi_y}^+ (z_0,z_m),$$

$$(39b)$$

and

$$\hat{X}_{\psi_y,\phi}^+ (z_m,z_m) = \hat{F}_{\psi_y,\psi_y}^- (z_m,z_0) X_{\psi_y,\phi}^+ (z_0,z_0) \hat{F}_{\phi,\phi}^+ (z_0,z_m). \quad (39c)$$

These equations describe redatuming of, respectively, the P-wave response, an S-wave response, and a converted response (P to S). Bear in mind that wave conversion is ignored only during propagation; wave conversion during reflection is fully accounted for. It is our experience that the advantage of independent redatuming more than counterbalances the disadvantage of ignoring wave conversion during propagation. For notational convenience, however, in the following we will stick to the more compact notation of Eq. (35).

Finally, we outline a complete imaging scheme, taking into account direct as well as indirect illumination of the

subsurface. In Eq. (35) we replace $\widehat{\mathbf{X}}_0^+(z_0,z_0)$ by $\widehat{\mathbf{X}}_{0,v}^+(z_0,z_0)$, i.e., the output of surface related pre-processing):

$$\widehat{\mathbf{X}}_{0,v}^+(z_m,z_m) = \widehat{\mathbf{F}}^-(z_m,z_0)\widehat{\mathbf{X}}_{0,v}^+(z_0,z_0)\widehat{\mathbf{F}}^+(z_0,z_m) \quad (40a)$$

or, using (32a),

$$\widehat{\mathbf{X}}_{0,v}^+(z_m,z_m) = \widehat{\mathbf{X}}_0^+(z_m,z_m) + \widehat{\mathbf{X}}_v^+(z_m,z_m), \quad (40b)$$

where

$$\widehat{\mathbf{X}}_0^+(z_m,z_m) = \widehat{\mathbf{F}}^-(z_m,z_0)\widehat{\mathbf{X}}_0^+(z_0,z_0)\widehat{\mathbf{F}}^+(z_0,z_m) \quad (40c)$$

and

$$\widehat{\mathbf{X}}_v^+(z_m,z_m) = \widehat{\mathbf{F}}^-(z_m,z_0)\widehat{\mathbf{X}}_v^+(z_0,z_0)\widehat{\mathbf{F}}^+(z_0,z_m). \quad (40d)$$

The propagation distorted contributions from $\mathbf{R}^+(z_k)$ for all $k \neq m$ as well as from $\widehat{\mathbf{X}}_v^+(z_m,z_m)$ can be suppressed by applying the generalized imaging procedure to $\widehat{\mathbf{X}}_{0,v}^+(z_m,z_m)$, yielding $\widehat{\mathbf{R}}^+(z_m)$.

Redatuming [Eqs. (40)] and generalized imaging should be carried out for $m = 1,...,M$. At z_M, the response matrix $\widehat{\mathbf{X}}_{0,v}^+(z_M,z_M)$ contains an anticausal term $\widehat{\mathbf{X}}_0^+(z_M,z_M)$ and a causal term $\widehat{\mathbf{X}}_v^+(z_M,z_M)$.

After removing the anticausal term (via the time domain), we are left with the indirect response $\widehat{\mathbf{X}}_v^+(z_M,z_M)$, which represents an estimate of

$$\mathbf{X}_v^+(z_M,z_M) = \mathbf{R}^+(z_M)\mathbf{X}^-(z_M,z_M)\mathbf{R}^+(z_M), \quad (41)$$

see Fig. 7.

Hence, we obtain an estimate of the virtual source response $\mathbf{X}^-(z_M,z_M)$ by inverting Eq. (41), according to

$$\widehat{\mathbf{X}}^-(z_M,z_M) = (\widehat{\mathbf{R}}^+(z_M))^{-1}\widehat{\mathbf{X}}_v^+(z_M,z_M)(\widehat{\mathbf{R}}^+(z_M))^{-1}. \quad (42)$$

The procedure may now be continued with multiple elimination by inverting Eq. (8b), according to

$$\widehat{\mathbf{X}}_0^-(z_M,z_M) = \widehat{\mathbf{X}}^-(z_M,z_M)$$
$$\times [\mathbf{I} + \widehat{\mathbf{R}}^+(z_M)\widehat{\mathbf{X}}^-(z_M,z_M)]^{-1}, \quad (43a)$$

(see also Fig. 6), followed by redatuming by inverting Eq. (7b), according to

$$\widehat{\mathbf{X}}_0^-(z_m,z_m) = \widehat{\mathbf{F}}^+(z_m,z_M)\widehat{\mathbf{X}}_0^-(z_M,z_M)\widehat{\mathbf{F}}^-(z_M,z_m) \quad (43b)$$

(see also Fig. 5) and generalized imaging, yielding $\widehat{\mathbf{R}}^-(z_m)$. Redatuming and generalized imaging should be carried out for $m = M - 1,...,1$.

C. Target related data fitting

The output of redatuming and imaging consists of a series of reflection matrices $\widehat{\mathbf{R}}^+(z_m)$ for $m = 1, ..., M$ and, optionally, $\widehat{\mathbf{R}}^-(z_m)$ for $m = 1,...,M - 1$. Any of these matrices consists of nine submatrices, according to

$$\widehat{\mathbf{R}}^+(z_m) = \begin{bmatrix} \widehat{\mathbf{R}}_{\phi,\phi}^+(z_m) & \widehat{\mathbf{R}}_{\phi,\psi_x}^+(z_m) & \widehat{\mathbf{R}}_{\phi,\psi_y}^+(z_m) \\ \widehat{\mathbf{R}}_{\psi_x,\phi}^+(z_m) & \widehat{\mathbf{R}}_{\psi_x,\psi_x}^+(z_m) & \widehat{\mathbf{R}}_{\psi_x,\psi_y}^+(z_m) \\ \widehat{\mathbf{R}}_{\psi_y,\phi}^+(z_m) & \widehat{\mathbf{R}}_{\psi_y,\psi_x}^+(z_m) & \widehat{\mathbf{R}}_{\psi_y,\psi_y}^+(z_m) \end{bmatrix}$$

$$(44a)$$

and

$$\widehat{\mathbf{R}}^-(z_m) = \begin{bmatrix} \widehat{\mathbf{R}}_{\phi,\phi}^-(z_m) & \widehat{\mathbf{R}}_{\phi,\psi_x}^-(z_m) & \widehat{\mathbf{R}}_{\phi,\psi_y}^-(z_m) \\ \widehat{\mathbf{R}}_{\psi_x,\phi}^-(z_m) & \widehat{\mathbf{R}}_{\psi_x,\psi_x}^-(z_m) & \widehat{\mathbf{R}}_{\psi_x,\psi_y}^-(z_m) \\ \widehat{\mathbf{R}}_{\psi_y,\phi}^-(z_m) & \widehat{\mathbf{R}}_{\psi_y,\psi_x}^-(z_m) & \widehat{\mathbf{R}}_{\psi_y,\psi_y}^-(z_m) \end{bmatrix}.$$

$$(44b)$$

Assuming that the generalized imaging procedure has been applied (paper II), any of the submatrices contains the angle-dependent reflection properties for a certain combination of incident and reflected wave types for all grid points at depth z_m. This information is used to determine the parameters of an interesting target zone by data fitting. Note that in the acoustic situation only P-wave reflection information is available, i.e., submatrix $\widehat{\mathbf{R}}_{\phi,\phi}^+(z_m)$. The extra information contained in the other submatrices in $\widehat{\mathbf{R}}^+(z_m)$ and, optionally, $\widehat{\mathbf{R}}^-(z_m)$, largely improves the obtainable resolution of the different parameters in the target zone.

IV. CONCLUSIONS

In this paper we extended the acoustic reflection imaging approach, developed in papers I and II, to the elastic situation. The main reason for employing an elastic reflection imaging technique is given by the fact that the medium parameters of the target can be better resolved from P- and S-reflection information than from P-reflection information alone. In paper II we already concluded that reflection imaging may be seen as one step of a full inversion process. The success of any inversion scheme depends largely on the transparency of the underlying forward model. The forward model that we developed in Sec. II appeals very well to physical intuition and all the essentials of elastic reflection experiments can be clearly recognized. Based on this forward model we developed a stepwise elastic inversion scheme (Sec. III). During surface related pre-processing the multi-component measurements are transformed into primary P- and S-wave responses. No prior information about the subsurface is required. Information about the source signature and the near surface parameters are obtained by making the preprocessing data adaptive. Once the data have been separated into primary P- and S-wave responses, the P- and S-wave propagation effects are eliminated independently, yielding angle-dependent P–P, P–S, S–P, and S–S reflection information of the target (generalized imaging). Knowledge of the macro subsurface model is essential in seismic exploration. Optionally the imaging is done via a strong bottom reflector (ultrasonic inspection). In the final step the angle-dependent reflection information is transformed into the detailed medium parameters of the target. The implementation and evaluation of the stepwise elastic inversion scheme is subject of ongoing research at the Laboratory of Seismics and Acoustics (Berkhout and Wapenaar[10]).

APPENDIX: ELASTIC TWO-WAY AND ONE-WAY WAVE FIELDS

The general relationship between elastic two-way and one-way wave fields at depth level z reads

$$\begin{bmatrix} \mathbf{V}(z) \\ \mathbf{T}(z) \end{bmatrix} = \begin{bmatrix} \mathbf{L}_1^+(z) & \mathbf{L}_1^-(z) \\ \mathbf{L}_2^+(z) & \mathbf{L}_2^-(z) \end{bmatrix} \begin{bmatrix} \mathbf{P}^+(z) \\ \mathbf{P}^-(z) \end{bmatrix} \qquad (A1a)$$

or, equivalently,

$$\begin{bmatrix} \mathbf{P}^+(z) \\ \mathbf{P}^-(z) \end{bmatrix} = \begin{bmatrix} \mathbf{N}_1^+(z) & \mathbf{N}_2^+(z) \\ \mathbf{N}_1^-(z) & \mathbf{N}_2^-(z) \end{bmatrix} \begin{bmatrix} \mathbf{V}(z) \\ \mathbf{T}(z) \end{bmatrix}, \qquad (A1b)$$

where

$$\mathbf{N}_1^\pm = [\mathbf{L}_1^\pm - \mathbf{L}_1^\mp (\mathbf{L}_2^\mp)^{-1} \mathbf{L}_2^\pm]^{-1}, \qquad (A1c)$$

$$\mathbf{N}_2^\pm = [\mathbf{L}_2^\pm - \mathbf{L}_2^\mp (\mathbf{L}_1^\mp)^{-1} \mathbf{L}_1^\pm]^{-1}. \qquad (A1d)$$

This equation is a generalization for arbitrary 3-D wave fields of equivalent plane wave expressions derived by amongst others Aki and Richards[11] or Kennett.[12] The wave field vectors $\mathbf{P}^+(z)$, $\mathbf{P}^-(z)$, $\mathbf{V}(z)$, and $\mathbf{T}(z)$ are discussed in Sec. II; for a discussion of the generalized operators $\mathbf{L}_1^\pm$, $\mathbf{L}_2^\pm$, $\mathbf{N}_1^\pm$, and $\mathbf{N}_2^\pm$ see Wapenaar et al.[6]

Equation (A1) is helpful for studying the behavior of one-way wave fields at boundaries. In Sec. II C we employed (A1) to derive the relation between the acquisition parameters and the one-way wave fields at the free surface. Here we use (A1) to derive reflection operators for one-way wave fields at an interface at $z = z_m$ between two homogeneous half-spaces. We use subscripts u and l to distinguish between the upper and the lower half-space. We consider two situations. For wave fields that are incident to the interface from above we define a reflection operator $\mathbf{R}^+(z_m)$ according to

$$\mathbf{P}_u^-(z_m) = \mathbf{R}^+(z_m)\mathbf{P}_u^+(z_m). \qquad (A2)$$

Using the boundary conditions $\mathbf{V}_u(z_m) = \mathbf{V}_l(z_m)$ and $\mathbf{T}_u(z_m) = \mathbf{T}_l(z_m)$ we obtain from (A1)

$$\mathbf{P}_l^-(z_m) = \sum_{\alpha=1}^{2} \mathbf{N}_{\alpha,l}^- [\mathbf{L}_{\alpha,u}^+ \mathbf{P}_u^+(z_m) + \mathbf{L}_{\alpha,u}^- \mathbf{P}_u^-(z_m)]. \qquad (A3)$$

Since $\mathbf{P}_l^-(z_m)$ equals zero for this situation we find upon substitution of (A2) into (A3)

$$\left(\sum_{\alpha=1}^{2} \mathbf{N}_{\alpha,l}^- \mathbf{L}_{\alpha,u}^-\right) \mathbf{R}^+(z_m)\mathbf{P}_u^+(z_m)$$

$$= -\left(\sum_{\alpha=1}^{2} \mathbf{N}_{\alpha,l}^- \mathbf{L}_{\alpha,u}^+\right) \mathbf{P}_u^+(z_m). \qquad (A4)$$

Since this equation should hold for any $\mathbf{P}_u^+(z_m)$ we obtain

$$\mathbf{R}^+(z_m) = -\left(\sum_{\alpha=1}^{2} \mathbf{N}_{\alpha,l}^- \mathbf{L}_{\alpha,u}^-\right)^{-1} \left(\sum_{\alpha=1}^{2} \mathbf{N}_{\alpha,l}^- \mathbf{L}_{\alpha,u}^+\right). \qquad (A5)$$

For wave fields that are incident to the interface from below we define a reflection operator $\mathbf{R}^-(z_m)$ according to

$$\mathbf{P}_l^+(z_m) = \mathbf{R}^-(z_m)\mathbf{P}_l^-(z_m). \qquad (A6)$$

Following the same approach as above we obtain

$$\mathbf{R}^-(z_m) = -\left(\sum_{\alpha=1}^{2} \mathbf{N}_{\alpha,u}^+ \mathbf{L}_{\alpha,l}^+\right)^{-1} \left(\sum_{\alpha=1}^{2} \mathbf{N}_{\alpha,u}^+ \mathbf{L}_{\alpha,l}^-\right). \qquad (A7)$$

Expressions (A5) and (A7) are strictly valid only for the situation of a horizontal interface at $z = z_m$ between two homogeneous half-spaces. Because the expressions are formulated in the space-frequency domain they are on principle suited to handle more complex configurations. Of course the accuracy decreases with increasing complexity of the configuration.

[1] A. J. Berkhout, "A unified approach to acoustical reflection imaging. I: The forward model," J. Acoust. Soc. Am. 93, 2005–2016 (1993).

[2] A. J. Berkhout and C. P. A. Wapenaar, "A unified approach to acoustical reflection imaging. II: The inverse problem," J. Acoust. Soc. Am. 93, 2017–2023 (1993).

[3] J. C. de Haas and A. J. Berkhout, "On the information content of P-P, P-SV, SV-SV, and SV-P reflections," in Proceedings of the 1988 International Meeting of the Society of Exploration Geophysicists (SEG, Anaheim, CA, 1988).

[4] C. Cliet and M. Dubesset, "Three component recordings: Interest for land seismic source study," Geophysics 52, 1048–1059 (1987).

[5] C. P. A. Wapenaar and A. J. Berkhout, Elastic Wave Field Extrapolation: Redatuming of Single- and Multi-component Seismic Data (Elsevier, Amsterdam, 1989).

[6] C. P. A. Wapenaar, P. Herrmann, D. J. Verschuur, and A. J. Berkhout, "Decomposition of multi-component seismic data into primary P and S wave responses," Geophys. Prospect. 38, 633–661 (1990).

[7] C. R. Smith and W. T. Grandy (Eds.), Maximum-Entropy and Bayesian Methods in Inverse Problems (Reidel, Dordrecht, 1985).

[8] D. J. Verschuur, A. J. Berkhout, and C. P. A. Wapenaar, "Wavelet estimation by prestack multiple elimination," in Proceedings of the 1989 International Meeting of the Society of Exploration Geophysicists (SEG, Dallas, TX, 1989).

[9] R. Versteeg and G. Grau (Eds.), "The Marmousi experience," in Proceedings of the 1990 EAEG Workshop on Practical Aspects of Seismic Inversion (EAEG, Copenhagen, 1990).

[10] A. J. Berkhout and C. P. A. Wapenaar, "Delphi: Delft philosophy on acoustic and elastic inversion," The Leading Edge 9(2), 30–33 (1990).

[11] K. Aki and P. G. Richards, Quantitative Seismology (Freeman, New York, 1980).

[12] B. L. N. Kennett, Seismic Wave Propagation in Stratified Media (Cambridge, U.P., Cambridge, 1983).

REFERENCES FOR GENERAL READING

W. F. Chang and G. A. McMechan, "Elastic reverse-time migration," Geophysics 52, 1365–1375 (1987).

S. H. Danbom and S. N. Domenico, Shear-Wave Exploration (Society of Exploration Geophysicists, Tulsa, 1987).

J. W. M. Dankbaar, "Separation of P and S waves," Geophys. Prospect. 33, 970–986 (1985).

S. K. Datta, J. D. Achenbach, and Y. S. Rajapakse (Eds)., "Elastic waves and ultrasonic nondestructive evaluation," in Proceedings of the IUTAM Symposium on Elastic Wave Propagation and Ultrasonic Evaluation (IUTAM, Boulder, CO, 1989).

G. Dohr (Ed.), Seismic Shear Waves (Geophysical Press, London, 1985).

J. T. Kuo and T. F. Dai, "Kirchhoff elastic wave migration for the case of non-coincident source and receiver," Geophysics 49, 1223–1238 (1984).

A. Tarantola, "A strategy for nonlinear elastic inversion of seismic reflection data," Geophysics 51, 1893–1903 (1986).